JACS
JOURNAL OF THE AMERICAN CHEMICAL SOCIETY
Article
pubs.acs.org/JACS

Observation of a Distinct Surface Molecular Orientation in Films of a High Mobility Conjugated Polymer

Torben Schuettfort,[†] Lars Thomsen,[‡] and Christopher R. McNeill*[,§]

[†]Cavendish Laboratory, University of Cambridge, JJ Thomson Avenue, Cambridge, CB3 0HE, U.K.
[‡]Australian Synchrotron, 800 Blackburn Road, Clayton, Victoria, 3168, Australia
[§]Department of Materials Engineering, Monash University, Wellington Road, Clayton, Victoria, 3800, Australia

Supporting Information

ABSTRACT: The molecular orientation and microstructure of films of the high-mobility semiconducting polymer poly(*N*,*N*-bis-2-octyldodecylnaphthalene-1,4,5,8-bis-dicarboximide-2,6-diyl-alt-5,5-2,2-bithiophene) (P(NDI2OD-T2)) are probed using a combination of grazing-incidence wide-angle X-ray scattering (GIWAXS) and near-edge X-ray absorption fine-structure (NEXAFS) spectroscopy. In particular a novel approach is used whereby the bulk molecular orientation and surface molecular orientation are simultaneously measured on the same sample using NEXAFS spectroscopy in an angle-resolved transmission experiment. Furthermore, the acquisition of bulk-sensitive NEXAFS data enables a direct comparison of the information provided by GIWAXS and NEXAFS. By comparison of the bulk-sensitive and surface-sensitive NEXAFS data, a distinctly different molecular orientation is observed at the surface of the film compared to the bulk. While a more "face-on" orientation of the conjugated backbone is observed in the bulk of the film, consistent with the lamella orientation observed by GIWAXS, a more "edge-on" orientation is observed at the surface of the film with surface-sensitive NEXAFS spectroscopy. This distinct edge-on surface orientation explains the high in-plane mobility that is achieved in top-gate P(NDI2OD-T2) field-effect transistors (FETs), while the bulk face-on texture explains the high out-of-plane mobilities that are observed in time-of-flight and diode measurements. These results also stress that GIWAXS lacks the surface sensitivity required to probe the microstructure of the accumulation layer that supports charge transport in organic FETs and hence may not necessarily be appropriate for correlating film microstructure and FET charge transport.

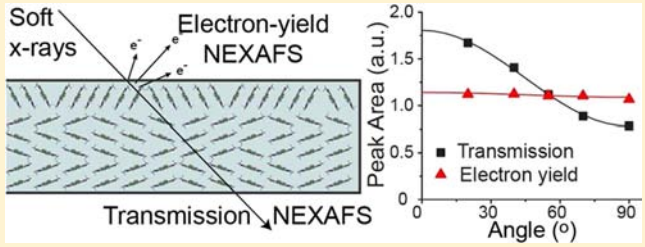

INTRODUCTION

Conjugated polymers are being intensely investigated for application in solution-processed organic field-effect transistors (OFETs).[1,2] The ability to solution-process the active layer of OFETs may enable low-cost flexible electronics via high-throughput printing techniques. In recent years a dramatic increase in the field-effect mobility of conjugated polymers has been observed, with reports of materials with mobilities of over 1 $cm^2/(V\ s)$ becoming more common.[3−6] While many different chemical motifs are now being employed in high mobility conjugated polymers,[2] a common feature is the use of alternating electron-rich and electron-poor units in so-called donor−acceptor copolymers.[6−8] Compared to thiophene- and thienothiophene-based conjugated polymers where improvements in charge transport mobilities have been linked with improvements in film microstructure,[9] the relationship between microstructure and charge transport mobility in these new high mobility donor−acceptor copolymers is not clear, with high mobilities accompanying both highly semicrystalline[10] and seemingly highly disordered films.[11] The establishment of structure/function relationships in OFETs is made more challenging by the fact that charge transport occurs along a thin, ∼1 nm thick accumulation layer at the semiconductor/dielectric interface.[12] Thus, microstructural characterization techniques should ideally have a surface sensitivity commensurate with the thickness of this thin, charge transporting surface layer.

The microstructure of organic semiconductor thin films used in OFETs is often characterized by grazing-incidence wide-angle X-ray scattering (GIWAXS)[13] (see Figure 1a for schematic). A grazing incidence geometry with a shallow angle of incidence minimizes background scattering from the substrate. This is achieved by using an angle of incidence, α_i, that is above the critical angle, α_c, of the organic semiconductor film but below the critical angle of the substrate. When $\alpha_i < \alpha_c$, total external reflection of the X-ray beam occurs with only an evanescent wave penetrating into the material. Going below the critical angle of the organic semiconductor affords GIWAXS near-surface sensitivity, with the penetration depth (the depth at which the X-ray beam is attenuated by $1/e$) in the limit of $\alpha_i \rightarrow 0$ given by[14]

$$\Lambda_0 = \lambda/(2\pi\alpha_c) \quad (1)$$

where λ is the wavelength of the X-ray beam. The critical angle α_c is given by[14]

Received: October 16, 2012
Published: December 25, 2012

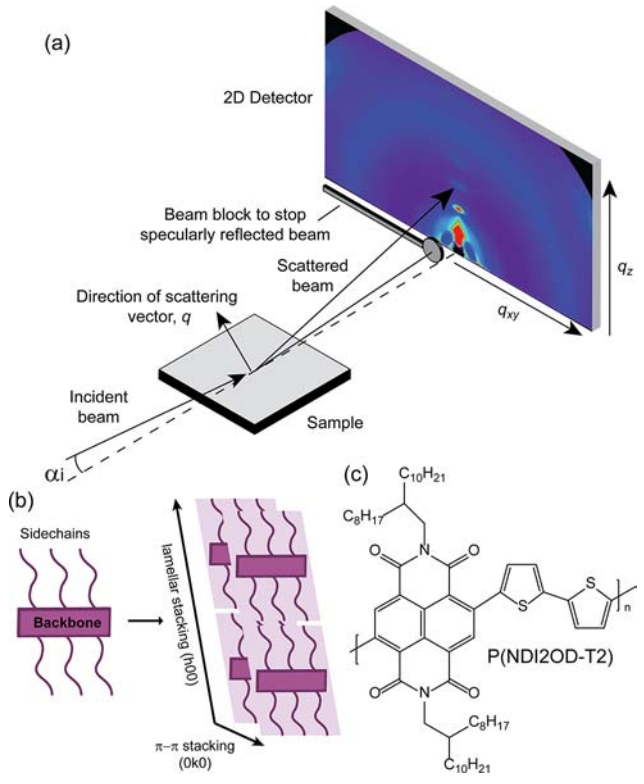

Figure 1. (a) Schematic diagram of a typical GIWAXS experimental setup. (b) Schematic representation of the packing of conjugated polymers to form lamellae. (c) Chemical structure of P(NDI2OD-T2).

$$\alpha_c = \lambda\sqrt{\frac{r_e\rho}{\pi}} \tag{2}$$

where r_e is the Thomson scattering length of the electron ($=2.817 \times 10^{-5}$ Å) and ρ is the electron density of the material. For conjugated polymers[15,16] $\rho \approx 0.4$ Å^{-3} and hence the critical angle for an X-ray energy of 14 keV is ~0.10°. Because of the appearance of λ in both eqs 1 and 2, the minimum penetration depth Λ_0 is independent of X-ray wavelength and is calculated to be $\Lambda_0 = 8.4$ nm for $\rho = 0.4$ Å^{-3}.

Performing GIWAXS measurements at a high brightness synchrotron source ensures sufficient scattering events with the in-plane and out-of-plane scattering from the sample recorded on a two-dimensional detector. Conjugated polymers with their planar backbones and long side chains can be regarded as "hairy", rigid-rod polymers and tend to pack in lamellae as shown schematically in Figure 1b. The $(h00)$ direction is indexed as the lamella stacking direction, the $(0k0)$ as the π–π-stacking direction, and the $(00l)$ direction as the polymer backbone direction. For polymer lamellae lying flat in the plane of the substrate the $(h00)$ scattering peaks appear along the q_{xy} direction, while for polymer lamella lying edge-on, $(h00)$ peaks appear along the q_z direction, as in Figure 1a. Although for conjugated polymer thin films there are typically not enough resolved diffraction peaks to uniquely determine the unit cell, GIWAXS has provided invaluable information regarding molecular packing, crystallite size, and crystallite orientation.[17−20]

Near-edge X-ray absorption fine-structure (NEXAFS) spectroscopy is another characterization technique for probing the molecular orientation of organic semiconductor thin films[21] (see Figure 2 for schematic). NEXAFS spectroscopy is a

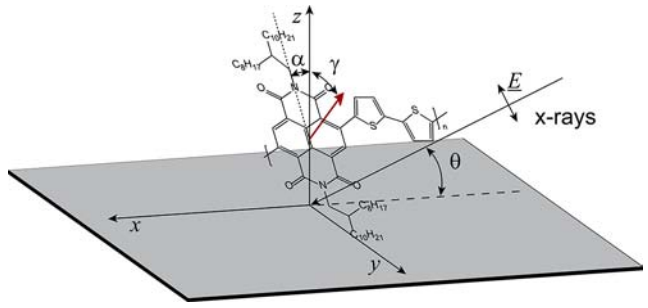

Figure 2. Schematic diagram of the geometry of an angle-resolved NEXAFS experiment. X-rays are incident on the sample subtending an angle θ to the substrate with the electric field vector parallel to the plane of incidence. The strength of a particular resonance is proportional to the projection of the electric field vector along the transition dipole moment (TDM), represented by the red arrow. The TDM subtends an angle γ to the surface normal and is perpendicular to the conjugation plane of the polymer backbone.

photon-absorbing spectroscopy associated with transitions from core states such as the C-1s state to antibonding molecular orbitals. The carbon K-edge NEXAFS spectrum of an organic semiconductor consists of peaks corresponding to resonant transitions from the carbon-1s core level to unoccupied molecular orbitals superimposed on the steplike absorption profile resulting from ionization. The lowest energy peaks found below the ionization step are typically the sharpest and are associated with transitions from C-1s orbitals to π^* antibonding orbitals. Since the resonance intensity of a particular transition is sensitive to the orientation of the transition dipole moment (TDM) of the transition with respect to the polarization of the incident X-ray beam, angle-resolved NEXAFS experiments can be used to determine the average tilt angle of a given TDM, γ. For aromatic structures the TDM of the C-1s → π^* transition is perpendicular to the ring-plane, and thus, angle-resolved NEXAFS experiments can also be used to determine the average tilt angle of the conjugated core of a conjugated polymer, α. By measurement of the absorption intensity of X-rays via so-called electron yield methods under ultrahigh vacuum, a surface sensitivity of 1−3 nm is achievable, commensurate with the depth of the accumulation in OFETs. The total electron yield (TEY) signal is recorded by measuring the current that flows from the sample to neutralize the charge due to secondary electrons leaving the film, while the Auger electron yield (AEY) signal is measured with a hemispherical energy analyzer directly detecting electrons that are ejected from the film with a specific kinetic energy. TEY has a surface sensitivity of 3 nm[22] with AEY having a superior surface sensitivity of ~1 nm[23] due to its ability to detect electron leaving with high kinetic energy. A weakness of NEXAFS spectroscopy, however, is that it is only able to determine an average tilt angle; when the measured average tilt is away from the two extremes (γ = 0°, 90°), it is difficult to distinguish preferential orientation at a particular angle from a large distribution of tilt angles.

Here we investigate the microstructure of thin films of the high-electron mobility conjugated polymer poly(*N*,*N*-bis-2-octyldodecylnaphthalene-1,4,5,8-bis-dicarboximide-2,6-diyl-alt-5,5-2,2-bithiophene) (P(NDI2OD-T2)[7] (see Figure 1c for structure). OFETs based on P(NDI2OD-T2) thin films exhibit electron mobilities of close to 1 cm^2/(V s) in top-gate transistors that are relatively insensitive to the way the film is processed.[7] P(NDI2OD-T2) films also exhibit an unconven-

dx.doi.org/10.1021/ja310240q | J. Am. Chem. Soc. 2013, 135, 1092−1101

tional microstructure with the polymer lamella in spin-coated films adopting a "face-on" orientation to the substrate as observed by GIWAXS.[24] Surface-sensitive angle-resolved near-edge X-ray absorption fine-structure (NEXAFS) spectroscopy measurements, on the other hand, return an average tilt angle of $\gamma \approx 55°$ corresponding to an average tilt angle of the polymer backbone of $\alpha = 35°$ from the surface normal.[25] This tilt angle would suggest a more edge-on orientation of the polymer lamella at the surface. However, because of the geometry of the experiment, this average tilt angle of $\gamma \approx 55°$ coincides with the so-called "magic angle" of 54.7°, which occurs for films lacking in-plane alignment of polymer chains[23] and thus could also reflect a random molecular orientation.[25] A disordered surface, however, seems inconsistent with recent evidence for the strong tendency of P(NDI2OD-T2) chains to aggregate in solution inhibiting the formation of amorphous and disordered P(NDI2OD-T2) films.[26]

A challenge associated with comparing GIWAXS and NEXAFS results is the different surface sensitivities of the two techniques, with GIWAXS being essentially a bulk technique and NEXAFS spectroscopy a highly surface sensitive technique. Therefore, to enable better comparison of GIWAXS and NEXAFS measurements, we have developed a novel angle-resolved transmission geometry enabling simultaneous measurement of transmission and electron-yield NEXAFS spectra (see Figure 3). Free-standing films are mounted on transmission electron microscopy (TEM) grids and mounted at an angle θ with respect to the incident electron beam. By placement of a photodiode behind the sample holder, the transmitted beam intensity can be measured simultaneous to the TEY and AEY signals. In this way, the molecular orientation of the surface and bulk of the same sample can be probed simultaneously with the same experimental technique. Furthermore, the acquisition of bulk-sensitive NEXAFS data enables a direct comparison of molecular orientation information returned by NEXAFS and GIWAXS. In this way we demonstrate that solution-cast P(NDI2OD-T2) films exhibit a surface molecular orientation that is distinct to the bulk molecular orientation. Furthermore, by measuring highly aligned P(NDI2OD-T2) films produced via the zone-casting technique that possess a different "magic angle" (45° instead of 54.7°),[23] we are able to show that the average surface tilt angle of $\gamma \approx 55°$ typically exhibited by P(NDI2OD-T2) films actually corresponds to a genuine preference for polymer chains at the surface to orient edge-on rather than reflecting a large amorphous fraction. These observations then permit a consistent microstructural explanation of bulk and surface charge transport phenomena previously observed in such films. Furthermore, the observation of a distinct surface orientation has significant implications for the way in which structure–function relationships in OFETs are established.

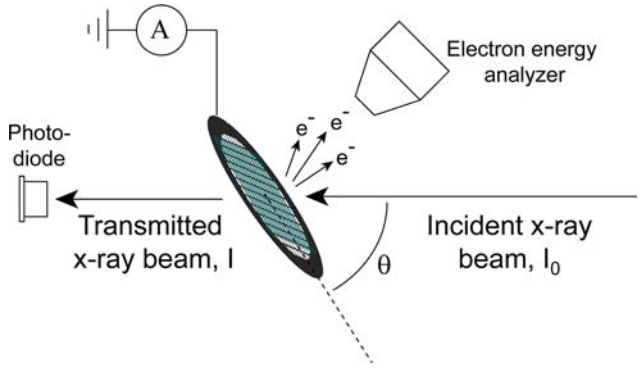

Figure 3. Schematic of the experimental setup enabling simultaneous angle-resolved transmission and electron-yield NEXAFS measurement.

EXPERIMENTAL SECTION

Sample Preparation. P(NDI2OD-T2) was purchased from Polyera Corp. (ActivInk N2200) with a specified number-average molecular weight (M_n) and polydispersity index (PDI) of 25.4 kDa and 4.03, respectively, as determined by the supplier with gel permeation chromatography using chloroform as the solvent. Silicon wafers were used as substrates precoated with a sacrificial layer of sodium polystyrene sulfonate (NaPSS) to aid float off. The use of NaPSS as a sacrificial layer did not affect the bulk or interfacial structure of P(NDI2OD-T2) films, with identical GIWAXS, electron yield NEXAFS, and atomic force microscopy results for films prepared on NaPSS and films prepared on conventionally treated silicon.[25] NaPSS was deposited by spin-coating from a 50 g/L solution in water before annealing at 150 °C for 30 min. Thin films of P(NDI2OD-T2) were prepared by spin-coating from a 20 g/L dichlorobenzene (DCB) solution in a nitrogen atmosphere to give films ~55 nm thick. An optional thermal annealing step was performed, either by annealing at 110 °C for 10 min and quenching to room temperature (as used in optimized transistors)[25] or by heating to 350 °C and slowly cooling to room temperature.[27] Films were delaminated from the substrate by floating off in deionized water and picking up on copper TEM grids (300 mesh with a transparency of 49%). The use of large substrates enabled half of the film to be floated off for NEXAFS measurement, leaving half of the film on the substrate for GIWAXS characterization. In this way the microstructure of the same film was characterized with multiple techniques. When used, octyltrichlorosilane (OTS) was deposited onto solvent- and O_2 plasma-cleaned silicon wafers from a hexane solution (0.2% vol) in a desiccator.

Zone-cast[28] films were deposited onto silicon wafers after oxygen plasma treatment. A 2 g L^{-1} P(NDI2OD-T2) DCB solution and the substrate were heated to 80 °C in nitrogen atmosphere. The solution was pushed through the nozzle using a syringe at 40 μm s^{-1}, while the substrate moved underneath the nozzle with a velocity of less than 30 μm s^{-1}.

Microstructural Characterization. NEXAFS spectroscopy was performed at the soft X-ray beamline at the Australian Synchrotron.[29] The AEY signal was recorded with a SPECS Phoibos 150 hemispherical analyzer set to a kinetic energy of 230 eV, while the TEY signal was recorded via the drain current through the sample with electron yield signals normalized to the incident photon flux using the "stable monitor method".[30] TEM grids were mounted onto the sample holder with conductive carbon tape to ensure electrical connectivity. Transmission spectra were acquired by measuring the transmitted photon flux with an AXUV100 photodiode from International Radiation Detectors, Inc., placed directly behind the sample holder. The measured transmitted X-ray intensity, I, was compared to the incident X-ray intensity, I_0, and converted to optical density via

$$\mathrm{OD} = \ln(I_0/I) \quad (3)$$

All NEXAFS spectra were normalized by subtracting the value at 280 eV and normalizing to the value at 320 eV. Fluorescence yield (FY) NEXAFS spectra were also simultaneously acquired using a multichannel plate fluorescence yield detector for comparison.

Grazing-incidence wide-angle X-ray scattering (GIWAXS) measurements were performed at the SAXS/WAXS beamline at the Australian Synchrotron. 14 keV photons were directed onto the sample to produce 2D scattering patterns recorded on an MAR-165 CCD detector. A grazing angle of 0.10° was used that is close to the critical angle of the polymer films (giving a penetration depth similar to the film thickness) but below the critical angle of the substrate. GIWAXS data were also taken as a function of angle of incidence to check for any changes with differing surface sensitivity. Further details of synchrotron experiments can be found in the Supporting Information.

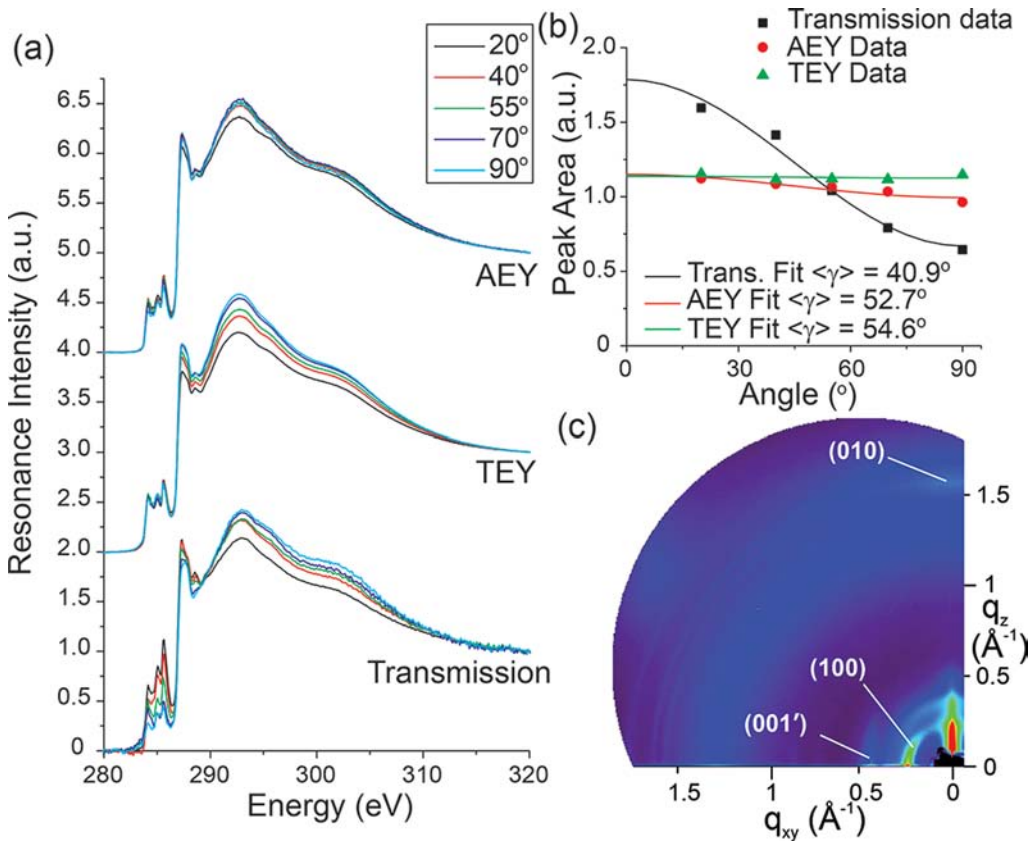

Figure 4. (a) Angle-resolved AEY, TEY, and transmission NEXAFS spectra of the as-cast P(NDI2OD-T2) film. (b) Plot of the area of the π^* manifold vs angle (points) with solid lines showing fits to the data. (c) 2D GIWAXS scattering pattern of the same film.

Atomic force microscopy (AFM) measurements were performed with either a Veeco Nanoscope IIIa or Nanoscope V in either noncontact or ScanAsyst mode.

RESULTS AND DISCUSSION

Figure 4a presents the angle-resolved NEXAFS spectra of the as-spun P(NDI2OD-T2) film simultaneously taken in AEY, TEY, and transmission modes. The shape of the AEY, TEY, and transmission spectra are all very similar when compared at an angle of incidence of 55° (see Supporting Information). The AEY and TEY spectra both show little dichroism over the region of 283−287 eV that corresponds to transitions from carbon-1s states to π^* antibonding states. The lack of dichroism in the π^* manifold is consistent with an average tilt angle of the transition dipole moment (TDM) of $\gamma \approx 55°$. Since the TDM is oriented perpendicular to the conjugated ring plane, an angle of $\gamma \approx 55°$ corresponds to a tilt angle of the conjugated backbone of $\alpha \approx 35°$ ($\alpha = 90° - \gamma$). Indeed, Figure 4b plots the area of the π^* manifold (determined via peak fitting; see Supporting Information) as a function of X-ray angle of incidence with solid lines showing fits to the data using the expression[23]

$$I = \frac{1}{3}\left[1 + \frac{1}{2}(3\cos^2\theta - 1)(3\cos^2\gamma - 1)\right] \quad (4)$$

where I is the resonance intensity, θ the angle of incidence, and γ the average tilt angle of the transition dipole moment.[23] For AEY detection an average tilt angle of $\alpha = 37.3° \pm 0.5°$ is determined ($\gamma = 52.7°$), while for TEY detection a similar tilt angle of $\alpha = 35.5° \pm 0.5°$ is found ($\gamma = 54.6°$). Note that in eq 4 the average tilt that is determined from fitting embodies both preferred orientation and the degree of orientational order which cannot easily be separated, especially for average tilt angles far from the two orientational extremes ($\gamma = 0°$, 90°). Indeed, the angles fitted above are all close to the so-called "magic-angle" ($\alpha = 35.3°$, $\gamma = 54.7°$) where the average tilt angle could correspond to a random distribution of tilt angles rather than an actual orientational preference.

A different situation is observed for the transmission data. Significant dichroism is observed for X-ray absorption at the π^* region. From a plot of the area of the π^* manifold as a function of X-ray angle of incidence and a fit to eq 4, an average tilt angle of $\alpha = 49° \pm 1°$ ($\gamma = 41°$) is returned. This value is significantly different from the magic angle, indicating a slightly face-on orientation of the polymer backbone. Interestingly this face-on orientational preference is in agreement with an average bulk tilt angle of $\alpha = 55°$ inferred from analysis of scanning transmission X-ray microscopy domain mapping data.[31] Similar enhanced dichroism of spin-coated P(NDI2OD-T2) thin films was also observed with fluorescence yield detection (see Supporting Information).

Figure 4c presents the 2D GIWAXS image of the as-spun film, with traces along q_{xy} and q_z provided in the Supporting Information. The GIWAXS measurements were taken of the same film used for NEXAFS measurement, using a portion of the film that was not floated off. The 2D GIWAXS image is similar to previous data taken on spin-coated P(NDI2OD-T2) films[24,25] with the (100) peak found predominantly along q_{xy} and the (010) $\pi-\pi$ stacking peak along q_z. (The lack of a (100) peak along q_z is more obvious from the projection along q_z shown in Figure S5.) The positions of the (100) and (010) peaks at $q_{xy} = 0.239$ Å^{-1} and $q_z = 1.60$ Å^{-1}, respectively, are

dx.doi.org/10.1021/ja310240q | J. Am. Chem. Soc. 2013, 135, 1092−1101

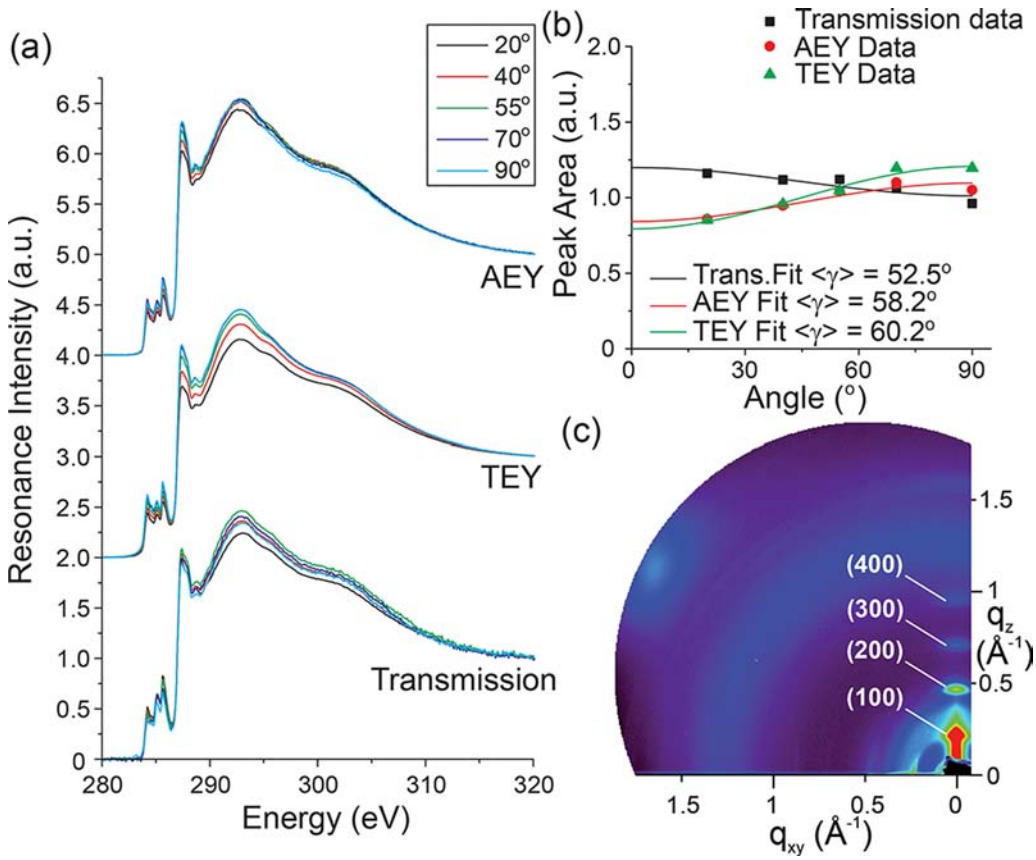

Figure 5. (a) Angle-resolved AEY, TEY, and transmission NEXAFS spectra of the P(NDI2OD-T2) film annealed to 340 °C and slowly cooled. (b) Plot of the area of the π^* manifold vs angle (points) with solid lines showing fits to the data. (c) 2D GIWAXS scattering pattern of the same film.

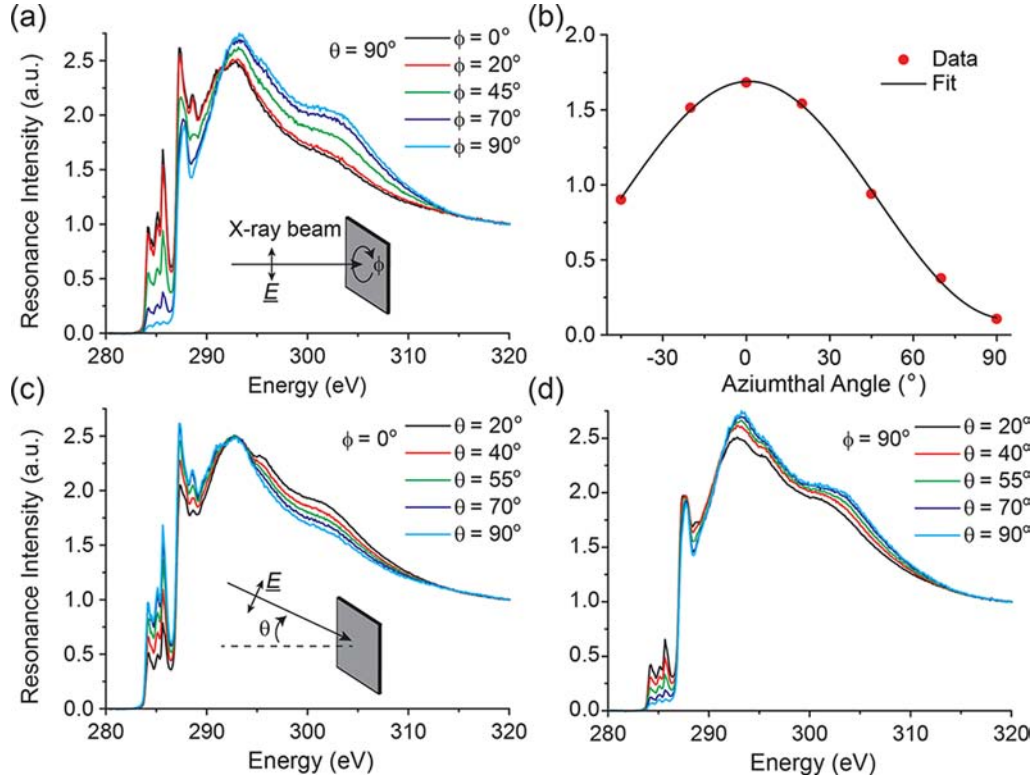

Figure 6. AEY NEXAFS spectra of aligned P(NDI2OD-T2) films produced by zone-casting. (a) Spectra acquired as a function of azimuthal angle with a normal angle of incidence. (b) Plot of peak area of the π^* manifold as a function of azimuthal angle with a fit to a cosine-squared function. (c) and (d) show NEXAFS spectra as a function of angle of incidence for an azimuthal angle of ϕ = 0° (c) and ϕ = 90° (d).

dx.doi.org/10.1021/ja310240q | J. Am. Chem. Soc. 2013, 135, 1092−1101

consistent with polymer lamella lying preferentially face-on to the substrate and an out-of-plane $\pi-\pi$ stacking direction,[24] in agreement with the bulk NEXAFS measurement. Such an orientation of polymer lamellae is not thought to be beneficial for in-plane charge transport (as in OFETs), since charge transport is efficient only along the polymer backbone and $\pi-\pi$ stacking directions, that is, the (001) and (010) directions.[18] GIWAXS measurements performed as a function of X-ray angle incidence from well-below the critical angle (0.04°) to above the critical angle (0.12°) showed identical scattering features indicating that GIWAXS is unable to discern differences in near-surface and bulk structure (see Supporting Information). GIWAXS and NEXAFS measurements performed on films annealed at 110 °C (the processing temperature that is commonly used in device fabrication) returned very similar results to those found for the as-spun film and can be found in the Supporting Information.

Figure 5 presents the NEXAFS and GIWAXS data for the P(NDI2OD-T2) film heated to above its melting point and slowly cooled to room temperature ("melt-annealed"). Such thermal treatment has been shown to result in a "drastic" change in the microstructure with the polymer lamellae changing from predominantly face-on to predominantly edge-on.[27] The GIWAXS pattern on the P(NDI2OD-T2) film heated to 340 °C and slowly cooled (Figure 5c) shows very different scattering features to the as-cast film in Figure 4 c, consistent with such a change. In particular, 4 orders of (h00) peaks are now observed along q_z. A weak (100) peak can still be observed along q_{xy}; however, the peak intensity is ∼17 times weaker than the (100) peak observed along q_z (see Supporting Information) consistent with >90% of crystallites[27] orienting edge-on to the substrate with in-plane $\pi-\pi$ stacking.

For the NEXAFS data (Figure 5a,b), this change in the bulk lamella orientation as observed by GIWAXS results in a change in the average bulk tilt-angle of the polymer backbone from α = 49° (γ = 40.9°) to α = 37° ± 1° (γ = 52.5°), confirming a change in average molecular orientation from preferentially face-on (α > 45°) to preferentially edge-on (α < 45°). Upon melt-annealing one may have expected a more dramatic change in bulk tilt angle as observed by transmission NEXAFS, an issue that will be returned to later in the discussion. At the surface of the film, the polymer chains adopt a slightly more edge-on orientation compared to the as-spun film, with average tilt angles of α = 31.7° ± 0.5° (γ = 58.2°) and α = 29.8° ± 0.5° (γ = 60.2°) measured using AEY and TEY modes, respectively.

While in all cases a preferential edge-on orientation is observed at the top surface of the film, that is, α < 45° (γ > 45°), since the measured tilt angles are close to the magic angle (α = 35.3°, γ = 54.7°), it is possible that the measured values reflect a random molecular orientation rather than a genuine orientational preference. In order to distinguish between these two cases, we have prepared biaxially aligned P(NDI2OD-T2) films via the zone-casting technique.[28] Here, the polymer solution is deposited onto a moving, heated substrate that produces aligned polymer backbones following the direction of solidification during solution coating. For films with in-plane alignment of the polymer backbone the magic-angle is changed to $\alpha = \gamma$ = 45°.[23]

Figure 6 presents the AEY NEXAFS spectra of the zone-cast P(NDI2OD-T2) film. Because of the biaxial alignment of the polymer chains, the NEXAFS spectra have to be recorded not just for different X-ray angles of incidence, θ, but also for different azimuthal angles, ϕ. Figure 6a shows the NEXAFS spectra recorded when probing the sample at normal incidence (θ = 90°) and then rotating from ϕ = 0° to ϕ = 90°. (ϕ = 0° corresponds to the geometry where the electric field vector of the X-ray beam is perpendicular to the zone-casting direction, while ϕ = 90° corresponds to where the electric field vector is parallel to the zone casting direction). While the conditions for film coating are different for zone-casting compared to spin-coating, our previous studies on PBTTT (poly(2,5-bis(3-tetradecylthiophen-2-yl)thieno[3,2-b]thiophene)) found identical surface tilt angles for spin-coated and zone-cast films.[32] Strong dichroism of the C-1s to π^* transition is observed consistent with a high degree of alignment of the polymer backbones, since the TDM of the C-1s to π^* transition is perpendicular to the P(NDI2OD-T2) backbone (regardless of the off-axis tilt angle). Figure 6b plots the peak area of the π^* manifold as a function of azimuthal angle, confirming that the X-ray absorption is varying as the cosine-squared of the azimuthal angle. The degree of dichroism can be quantified using the expression

$$D = \frac{A_{\parallel} - A_{\perp}}{A_{\parallel} + A_{\perp}} \tag{5}$$

where $A_{\parallel}$ and $A_{\perp}$ are the peak areas corresponding to when the electric field vector is parallel or perpendicular to the zone-casting direction, respectively. In this way a dichroism of D = 0.86 ± 0.01 is determined. Interestingly this surface dichroism value is significantly higher than that determined for zone-cast and annealed PBTTT films where a value of D = 0.73 was found.[32] Thus, the zone-casting of P(NDI2OD-T2) produces films with highly aligned surfaces. In contrast to PBTTT films, however, annealing of zone-cast P(NDI2OD-T2) films was found to destroy the backbone alignment even for very short anneal times. GIWAXS measurements of the zone-cast film confirm a high degree of in-plane alignment in the bulk of the film, similar to GIWAXS measurements performed on aligned films produced by dip-coating.[24] (GIWAXS data of the zone-cast film can be found in the Supporting Information.)

Figure 6c and Figure 6d present the NEXAFS spectra as a function of X-ray angle of incidence, θ, for ϕ = 0° (Figure 6c) and ϕ = 90° (Figure 6d). For the case of 2-fold rotational symmetry, such as in aligned polymer films, the relationship between the tilt angle of the TDM, γ, and angles θ and ϕ is[23]

$$I = \cos^2\gamma\cos^2\theta + \sin^2\gamma\sin^2\theta\cos^2\varphi \tag{6}$$

Using eq 6, the average tilt angle of the transition dipole moment is determined to be γ = 57.5° ± 0.5°. This value corresponds to a surface tilt angle of the conjugated backbone of α = 32°, similar to values found above. However, for this case where there is in-plane alignment of the polymer chains the magic angle is now $\gamma = \alpha$ = 45°.[23] Thus, the observed tilt angle is significantly away from the magic angle, reflecting a genuine preference for the polymer backbone to orient edge-on. It can therefore be argued that for the spin-coated films the measured tilt angles also reflect a genuine edge-on orientational preference as opposed to a disordered surface structure. Our conclusion, that P(NDI2OD-T2) chains are actually orienting edge-on at the surface rather than being disordered, is also consistent with evidence that P(NDI2OD-T2) chains aggregate in solution making the formation of amorphous films unlikely for P(NDI2OD-T2).[26]

The observation of a preferentially edge-on surface orientation at the top surface of P(NDI2OD-T2) films helps

to explain the observed charge transport phenomena in P(NDI2OD-T2) films. In particular, a distinct surface to bulk orientation explains how such films are able to simultaneously support high out-of-plane (as observed by time-of-flight[33] and space-charge-limited diode measurements[33,34]) and in-plane (as measured in an OFET experiment[7]) charge transport mobilities. In an OFET, charge transport occurs within the thin accumulation layer that is localized to within a few nanometers of the semiconductor dielectric interface. While the microstructure of this thin surface layer is critical for charge transport in an OFET, it is not likely to significantly affect charge transport through the bulk of the film where charges have to travel 100−1000 nm in thicker films used for time-of-flight and space-charge-limited diode measurements.

For melt-annealed films, the change in bulk lamella orientation from predominantly face-on to predominately edge-on was found to result in a 6-fold decrease in bulk current density.[27] In contrast, the OFET mobility measured in bottom-gate top-contact FETs was only found to decrease by 27%, leading the authors to conclude that the morphological changes that occur during melt-annealing are either not present at the interface or not the limiting factor for in-plane charge transport.[27] Our observation that surface microstructure can be distinct to the bulk microstructure supports the conclusion that the morphological changes in the bulk and at the interface are different. Although we have probed the structure of the top surface as relevant for top-gate devices, we found that while the average bulk tilt angle changes from $\alpha = 49.1°$ to $\alpha = 37.6°$ (a change of ∼12°), the average surface tilt angle changes by only ∼5° from ∼36° to 31°. Moreover, the bulk change in orientation corresponds to a change from preferentially face-on to preferentially edge-on, while the surface change corresponds to the orientation becoming more edge-on. Interestingly our previous measurement[25] of the surface orientation of the bottom of films prepared on bare silicon found a tilt angle of $\alpha \approx 50°$, suggesting that for films prepared on oxygen plasma-treated silicon the molecular orientation of the bottom surface is similar to that of the bulk for as-cast films.[25] Bottom-gate transistors using SiO_2 as the dielectric utilize an octadecyltrichlorosilane (OTS) layer to improve transistor performance[24] that passivates the electron-trapping hydroxyl groups on the SiO_2 surface.[35] The use of an OTS layer, however, is also known to affect interfacial molecular orientation.[36] However, similar to the measurements of the films discussed above, the bottom surface of OTS films also exhibits a preferred edge-on tilt angle of $\gamma = 50°$ of the backbone (see Supporting Information). Thus, it appears that for high performance bottom-gate transistors using OTS-passivated SiO_2 the interfacial morphology is also distinct to the bulk morphology.

Our observation of the top surface of P(NDI2OD-T2) films showing a preferential edge-on orientation after solution processing is consistent with phenomenon observed in other high performance conjugated polymer films. For PBTTT films, highly edge-on tilt angles of $\alpha = 23°$ are observed at the top surface of spin-coated films even before annealing into the more ordered terraced morphology.[32] After annealing, the tilt angle decreases only to $\alpha = 21°$,[32] despite the large changes in bulk microstructure with annealing as revealed by GIWAXS.[19] In particular, GIWAXS measurements of as-cast PBTTT films show a large proportion of crystallites with their (100) unit cell axis misaligned from the surface normal, while after annealing little misorientation remains.[19] The apparent different surface and bulk orientational behavior of PBTTT films suggests the presence of distinct surface and bulk microstructure in these films as well (at least for as-cast films). For poly(3-alkylthiophene) (P3AT), different molecular orientations have also been observed for the top and bottom surfaces of the film.[21]

The tendency for as-cast films to form face-on crystallites can be understood in terms of the strong tendency of P(NDI2OD-T2) chains to aggregate in solution. A recent study by Steyrleuthner et al.[26] presented photophysical evidence for the aggregation of P(NDI2OD-T2) chains in solution. Aggregation was found to proceed in solution via the coiling of individual polymer chains with film formation governed by the chain collapse leading in general to a high aggregate content of ∼45%. The formation of face-on lamellae may then be attributed to the flattening of the globuli during spin-coating and drying.[26] Shorter polymer chains, however, are less likely to aggregate and will be more soluble than longer molecular weight chains. The rather high polydispersity (PDI = 4.0) of our P(NDI2OD-T2) batch (similar to that used by others[7,26,27]) means that there will be a significant low molecular weight fraction that does not aggregate prior to film formation which we hypothesize is deposited at the surface of the film. Interestingly the surface morphology of the as-cast, melt-annealed, and zone-cast films all show different surface morphologies (see Figure 7), despite exhibiting similar surface tilt angles ($\alpha \approx 33° \pm 3°$) and bulk crystal grain size (20 ± 2 nm, as determined from Scherrer analysis of the width of the (100) peak). This observation suggests that while the precise surface morphology

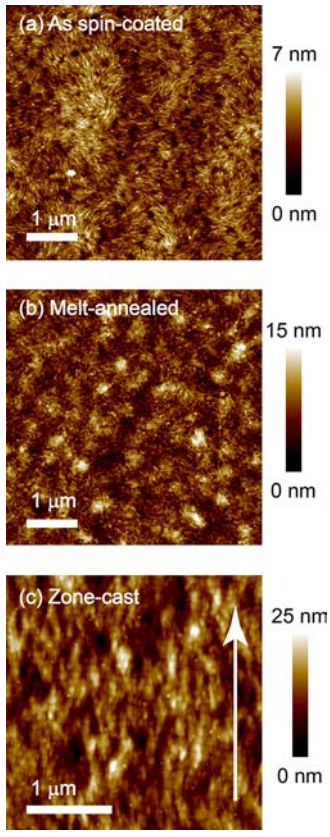

Figure 7. Atomic force microscopy images of the surface topography of (a) as-cast, (b) melt-annealed, and (c) zone-cast films. The arrow in (c) indicates the zone-casting direction.

of the top of the film is affected by the film drying conditions, all films nonetheless adopt a similar edge-on surface orientation, consistent with results from the PBTTT system where similar surface tilt angles are observed independent of surface morphology.[32] Furthermore, the formation of P(NDI2OD-T2) films with preferential edge-on orientation independent of substrate and solution processing route explains the observation of high-performance top-gate transistors fabricated on different substrates by a range of deposition techniques (spin-coating, gravure, flexographic, and inkjet printing).[7]

Given the assertion that the performance of P(NDI2OD-T2) OFETs is sensitive to surface molecular orientation, one may wonder why more pronounced tilt angles and changes in tilt angle are not observed. First, it should be noted that even for highly ordered PBTTT films where the (100) unit cell axis is oriented perpendicular to the substrate,[19] a tilt angle of the conjugated backbone of $\alpha = 21°$ from the surface normal is measured.[37] In this case the deviation of the backbone tilt angle from the surface normal is due to the conjugated backbone being tilted within the unit cell itself.[37] That is, the orientation of the (100) crystal axis and the tilt angle of the backbone are not necessarily the same. Indeed, backbone tilt angles of $\alpha = 21-30°$ are common for semicrystalline conjugated polymer films.[38,39] Second, while GIWAXS probes the orientation of the unit cell axes of coherent crystallites, NEXAFS is equally sensitive to ordered and disordered polymer chains. Thus, the tilt angles measured by NEXAFS reflect average tilt angles, and an amorphous fraction will reduce the average tilt angle to closer to the magic angle. Indeed in our previous study we attributed the measured tilt angles of $\gamma \approx 55°$ in spin-coated P(NDI2OD-T2) films to a large amorphous fraction.[25] However, here we discount this possibility because of the observation of similar tilt angles in biaxially aligned films (which possess a different magic angle) and recent evidence from other groups indicating that the formation of amorphous structure is less likely.[26]

Notably, the presence of a large dihedral angle between the naphthalene diimide (NDI) and thiophene (T2) units will result in less pronounced tilt angles. As isolated molecular species, the NDI and T2 units will have transition dipole moments as indicated schematically in Figure 8. In the absence of any significant wave function overlap the NEXAFS spectrum of P(NDI2OD-T2) can be thought of as the sum of the NEXAFS spectra of the NDI and T2 subunits. In such a case the different peaks in the π^* manifold can be attributed to different chemical species with the lower energy peaks associated with the high electron affinity NDI unit and the peak at ~285.5 eV associated with the thiophene moiety. It would then be expected that in the presence of significant torsion between the NDI and T2 moieties (as predicted by theoretical studies[40]) different tilt angles should be measured for the different peaks in the π^* manifold. However, in the case of the zone-cast samples where significant dichroism is observed, all peaks in the π^* manifold give an almost identical value for the average tilt angle. Thus, the TDMs corresponding to 1s to π^* transitions have contributions from both NDI and T2 moieties due to wave function overlap (we note that the LUMO is not completely localized on the NDI unit[40]). Since all peaks in the π^* manifold exhibit almost identical dichroism, the orientation of the measured π^* TDMs in a simplistic first-order approximation can then be thought of as the vector sum of the individual NDI and T2 TDMs, weighted by the number

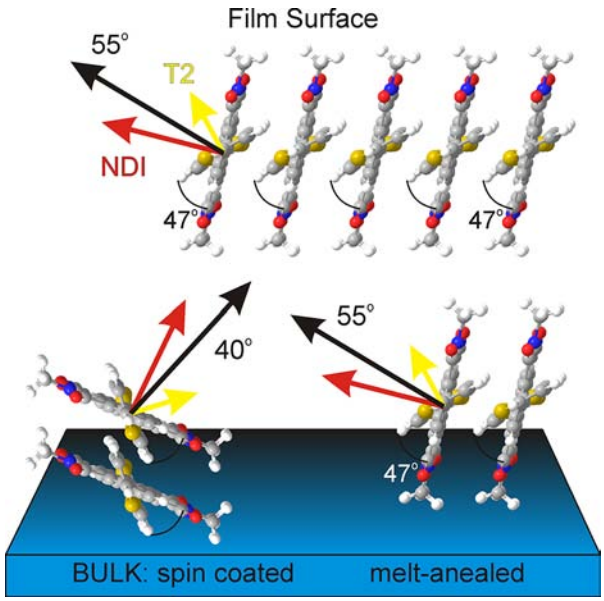

Figure 8. Schematic showing likely molecular orientations at the surface and bulk based on the measured values of the overall TDM (black arrow). Also represented is the relationship between the orientation of the measured TDM and the orientation of the individual TDMs of the naphthalene diimide (NDI, red) and thiophene (T2, yellow) units for a dihedral angle of 47°. Note that only the NDI and T2 cores are shown; the side chains that are tethered to the NDI units are omitted for clarity.

of carbon atoms on each moiety and the oscillator strength at the particular energy. Figure 8 schematically shows the relationship between the orientation of the measured TDM and that of the individual TDMs of the NDI and T2 units in the presence of a dihedral angle of ~47° as determined by quantum chemical calculations.[25,40] For a given tilt of the averaged TDM, there exist two molecular configurations: one with the NDI unit more edge-on to the substrate and one with the NDI unit more face-on (see Supporting Information for examples). For the case of the as-spun film a bulk average tilt angle of $\gamma = 41°$ observed. Since a dominant face-on bulk packing of crystallites is observed from GIWAXS, the orientation with the NDI unit more face-on in the bulk is most probable (see Figure 8), since the side chains are tethered to the NDI unit. For the case of the melt-annealed film, a bulk average tilt angle of $\gamma = 53°$ is observed with the lamella stacking edge-on to the substrate as observed by GIWAXS. Thus, for the melt-annealed film, the configuration with NDI unit more edge-on in the bulk is more probable, as shown in Figure 8. Thus, the observed change in the bulk average tilt angle of $\gamma = 41°$ to $\gamma = 53°$ is likely to actually correspond to a change in the average tilt angle of the isolated NDI TDM from $\gamma_{NDI} \approx 24°$ to $\gamma_{NDI} = 69°$ (since the overall TDM subtends an angle of 16.5° to the TDM of the NDI unit for a dihedral angle of 47°). Such a dramatic change in molecular orientation would be more consistent with the dramatic change in lamellae orientation observed with GIWAXS. For the surface of the film the lack of GIWAXS data with commensurate surface sensitivity to electron-yield NEXAFS does not permit the preferred configuration at the surface to be as easily discerned. However, given that the lowest unoccupied molecular orbital is predominantly localized on the NDI unit[40] (with the LUMO arguably more important for electron transport) and that the top surface of the film consistently supports high charge

dx.doi.org/10.1021/ja310240q | J. Am. Chem. Soc. 2013, 135, 1092−1101

transport mobilities in top-gate devices, the configuration with the NDI unit more edge-on certainly seems more plausible. Indeed it is likely that only this geometry is able to explain the high mobilities achievable by high performance top-gate P(NDI2OD-T2) transistors.

The observation of a distinct surface molecular orientation has significant ramifications for microstructure/charge transport studies of conjugated polymer films in general. GIWAXS has become a standard technique for determining and relating molecular orientation to OFET charge transport behavior.[41] As shown here, a different surface molecular orientation is detected with surface-sensitive NEXAFS spectroscopy to the dominant bulk molecular orientation that is detected by GIWAXS and bulk NEXAFS spectroscopy. Since charge transport in an OFET occurs within the ∼1 nm thick accumulation layer localized at the semiconductor/dielectric interface, techniques must be employed that have a commensurate surface sensitivity. The fact that GIWAXS is unable to detect any difference in the bulk and near-surface structure indicates that even when probing with an angle of incidence below the critical angle of the film, GIWAXS still lacks the required surface sensitivity that is obtained with electron-yield NEXAFS spectroscopy. Thus, there is the possibility for drawing erroneous conclusions when using GIWAXS alone to infer the molecular orientation as important for OFET charge transport. While X-ray scattering is a powerful technique for probing the crystalline structure of semicrystalline polymer films, one must be wary when using GIWAXS in isolation to draw conclusions regarding surface structure and hence the relationship between film microstructure and charge transport in an OFET. Equally, the use of NEXAFS to unambiguously determine molecular orientation is hampered by the lack of clear information regarding the distribution of molecular orientations. As employed here, the combination of GIWAXS with bulk and surface sensitive NEXAFS provides a more complete picture of molecular ordering in conjugated polymer films and provides a consistent explanation for the bulk and interfacial charge transport phenomena in P(NDI2OD-T2) films.

CONCLUSIONS

Angle-resolved NEXAFS experiments have been performed on a high-mobility conjugated polymer in transmission and surface-sensitive modes, enabling a direct comparison with molecular orientation information provided by GIWAXS. We observe a distinct edge-on preferential orientation of the conjugated polymer backbone at the surface of spin-coated P(NDI2OD-T2) films with an average tilt angle of the backbone of $\alpha \approx 36°$ from the surface normal in contrast to the bulk face-on molecular orientation observed by GIWAXS and transmission NEXAFS (where α is approximately 50°). Melt-annealing to produce an edge-on bulk texture is found to result in a change in the bulk tilt angle from $\alpha \approx 50°$ to $\alpha \approx 38°$ and a decrease in the surface tilt angle to $\alpha \approx 31°$. Highly aligned P(NDI2OD-T2) films have also been produced by zone-casting, confirming that the measured surface tilt angles correspond to a genuine preferential edge-on orientation. The observation of a distinct edge-on surface orientation in spin-coated P(NDI2OD-T2) accounts for the high charge transport mobilities observed in top-gate transistors. Furthermore, the observed in-plane bulk molecular orientation enables high out-of-plane charge transport mobilities to be supported. These results also show that caution must be used when using GIWAXS or NEXAFS in isolation to draw conclusions regarding molecular orientation and highlight the power of combining complementary techniques.

ASSOCIATED CONTENT

Supporting Information

Full details of synchrotron experiments; comparison of the shape of transmission and electron-yield NEXAFS spectra; fluorescence-yield NEXAFS data; details of NEXAFS peak fitting; GIWAXS data as a function of angle of incidence; GIWAXS traces along q_{xy} and q_z; microstructural characterization of the 110 °C annealed film; GIWAXS data of the zone-cast film; angle-resolved AEY NEXAFS spectra of P(NDI2OD-T2) on OTS-treated silicon. This material is available free of charge via the Internet at http://pubs.acs.org.

AUTHOR INFORMATION

Corresponding Author

christopher.mcneill@monash.edu

Notes

The authors declare no competing financial interest.

ACKNOWLEDGMENTS

We gratefully acknowledge funding from the Australian Research Council (ARC, Grant FT100100275), the Victorian Endowment for Science Knowledge and Innovation (VESKI), and the Engineering and Physical Sciences Research Council (EPSRC, Grant EP/E051804/1). The authors thank Nigel Kirby of the Australian Synchrotron for assistance with GIWAXS measurements, and Roland Resel of TU Graz for discussions. T.S. thanks Mijung Lee for assistance with the preparation of zone-cast samples. This research was undertaken on the soft X-ray and SAXS/WAXS beamlines at the Australian Synchrotron, Australia. This work was also performed in part at the Melbourne Centre for Nanofabrication.

REFERENCES

(1) Wang, C.; Dong, H.; Hu, W.; Liu, Y.; Zhu, D. *Chem. Rev.* **2011**, *112*, 2208.
(2) Facchetti, A. *Chem. Mater.* **2011**, *23*, 733.
(3) Lei, T.; Dou, J.-H.; Pei, J. *Adv. Mater.* **2012**, *24*, 6457.
(4) Fan, J.; Yuen, J. D.; Cui, W.; Seifter, J.; Mohebbi, A. R.; Wang, M.; Zhou, H.; Heeger, A.; Wudl, F. *Adv. Mater.* **2012**, *24*, 6164.
(5) Wang, S.; Kappl, M.; Liebewirth, I.; Müller, M.; Kirchhoff, K.; Pisula, W.; Müllen, K. *Adv. Mater.* **2012**, *24*, 417.
(6) Nielsen, C. B.; Turbiez, M.; McCulloch, I. *Adv. Mater.* **2013**, DOI: 10.1002/adma.201201795.
(7) Yan, H.; Chen, Z.; Zheng, Y.; Newman, C.; Quinn, J. R.; Dötz, F.; Kastler, M.; Facchetti, A. *Nature* **2009**, *457*, 679.
(8) Tsao, H. N.; Cho, D.; Andreasen, J. W.; Rouhanipour, A.; Breiby, D. W.; Pisula, W.; Müllen, K. *Adv. Mater.* **2009**, *21*, 209.
(9) McCulloch, I.; Heeney, M.; Chabinyc, M. L.; DeLongchamp, D.; Kline, R. J.; Coelle, M.; Duffy, W.; Fischer, D.; Gundlach, D.; Hamadani, B.; Hamilton, R.; Richter, L.; Salleo, A.; Shkunov, M.; Sporrowe, D.; Tierney, S.; Zhong, W. *Adv. Mater.* **2009**, *21*, 1091.
(10) Kronemeijer, A. J.; Gili, E.; Shahid, M.; Rivnay, J.; Salleo, A.; Heeney, M.; Sirringhaus, H. *Adv. Mater.* **2012**, *24*, 1558.
(11) Liu, J.; Zhang, R.; Sauvé, G.; Kowalewski, T.; McCullough, R. D. *J. Am. Chem. Soc.* **2008**, *130*, 13167.
(12) Horowitz, G. *Adv. Mater.* **1998**, *10*, 365.
(13) Rivnay, J.; Mannsfeld, S. C. B.; Miller, C. E.; Salleo, A.; Toney, M. F. *Chem. Rev.* **2012**, *112*, 5488.
(14) Tolan, M. *X-ray Scattering from Soft-Matter Thin Films*; Springer-Verlag, Berlin, 1999.

(15) Parnell, A. J.; Cadby, A. J.; Mykhaylyk, O. O.; Dunbar, A. D. F.; Hopkinson, P. E.; Donald, A. M.; Jones, R. A. L. *Macromolecules* **2011**, *44*, 6503.
(16) Chiu, M. Y.; Jeng, U. S.; Su, C. H.; Liang, K. S.; Wei, K. H. *Adv. Mater.* **2008**, *20*, 2573.
(17) Kline, R. J.; McGehee, M. D.; Toney, M. F. *Nat. Mater.* **2006**, *5*, 222.
(18) Sirringhaus, H.; Brown, P. J.; Friend, R. H.; Nielsen, M. M.; Bechgaard, K.; Langeveld-Voss, B. M. W.; Spiering, A. J. H.; Janssen, R. A. J.; Meijer, E. W.; Herwig, P.; de Leeuw, D. M. *Nature* **1999**, *401*, 685.
(19) Chabinyc, M. L.; Toney, M. F.; Kline, R. J.; McCulloch, I.; Heeney, M. *J. Am. Chem. Soc.* **2007**, *129*, 3226.
(20) Himmelberger, S.; Dacuña, J.; Rivnay, J.; Jimison, L. H.; McCarthy-Ward, T.; Heeney, M.; McCulloch, I.; Toney, M. F.; Salleo, A. *Adv. Funct. Mater.* **2013**, DOI: 10.1002/adfm.201202408.
(21) McNeill, C. R.; Ade, H. *J. Mater. Chem. C* **2013**, *1*, 187.
(22) Chua, L.-L.; Dipankar, M.; Sivaramakrishnan, S.; Gao, X.; Qi, D.; Wee, A. T. S.; Ho, P. K. H. *Langmuir* **2006**, *22*, 8587.
(23) Stöhr, J. *NEXAFS Spectroscopy*; Springer: Berlin, 1992.
(24) Rivnay, J.; Toney, M. F.; Zheng, Y.; Kauvar, I. V.; Chen, Z.; Wagner, V.; Facchetti, A.; Salleo, A. *Adv. Mater.* **2010**, *22*, 4359.
(25) Schuettfort, T.; Huettner, S.; Lilliu, S.; Macdonald, J. E.; Thomsen, L.; McNeill, C. R. *Macromolecules* **2011**, *44*, 1530.
(26) Steyrleuthner, R.; Schubert, M.; Howard, I. A.; Klaumünzer, B.; Schilling, K.; Chen, Z.; Saalfrank, P.; Laquai, F.; Facchetti, A.; Neher, D. *J. Am. Chem. Soc.* **2012**, *134*, 18303.
(27) Rivnay, J.; Steyrleuthner, R.; Jimison, L. H.; Casadei, A.; Chen, Z.; Toney, M. F.; Facchetti, A.; Neher, D.; Salleo, A. *Macromolecules* **2011**, *44*, 5246.
(28) Tang, C.; Tracz, A.; Kruk, M.; Zhang, R.; Smilgies, D.-M.; Matyjaszewski, K.; Kowalewski, T. *J. Am. Chem. Soc.* **2005**, *127*, 6918.
(29) Cowie, B. C. C.; Tadich, A.; Thomsen, L. *AIP Conf. Proc.* **2010**, *1234*, 307.
(30) Watts, B.; Thomsen, L.; Dastoor, P. C. *J. Electron Spectrosc. Relat. Phenom.* **2006**, *151*, 105.
(31) Sciascia, C.; Martino, N.; Schuettfort, T.; Watts, B.; Grancini, G.; Antognazza, M. R.; Zavelani-Rossi, M.; McNeill, C. R.; Caironi, M. *Adv. Mater.* **2011**, *23*, 5086.
(32) Schuettfort, T.; Watts, B.; Thomsen, L.; Lee, M.; Sirringhaus, H.; McNeill, C. R. *ACS Nano* **2012**, *6*, 1849.
(33) Steyrleuthner, R.; Schubert, M.; Jaiser, F.; Blakesley, J. C.; Chen, Z.; Facchetti, A.; Neher, D. *Adv. Mater.* **2010**, *22*, 2799.
(34) Caironi, M.; Newman, C.; Moore, J. R.; Natali, D.; Yan, H.; Facchetti, A.; Sirringhaus, H. *Appl. Phys. Lett.* **2010**, *96*, 183303.
(35) Chua, L.-L.; Zaumseil, J.; Chang, J. F.; Ou, E. C.-W.; Ho, P. K.-H.; Sirringhaus, H.; Friend, R. H. *Nature* **2005**, *434*, 194.
(36) Kline, R. J.; DeLongchamp, D. M.; Fischer, D. A.; Lin, E. K.; Heeney, M.; McCulloch, I.; Toney, M. F. *Appl. Phys. Lett.* **2007**, *90*, 062117.
(37) DeLongchamp, D. M.; Kline, R. J.; Lin, E. K.; Fischer, D. A.; Richter, L. J.; Lucas, L. A.; Heeney, M.; McCulloch, I.; Northrop, J. E. *Adv. Mater.* **2007**, *19*, 833.
(38) Oosterbaan, W.; Bolsée, J.-C.; Gadisa, A.; Vrindts, V.; Bertho, S.; D'Haen, J.; Cleij, T. J.; Lutsen, L.; McNeill, C. R.; Thomsen, L.; Manca, J. V.; Vanderzande, D. *Adv. Funct. Mater.* **2010**, *20*, 792.
(39) Zhang, X.; Richter, L. J.; DeLongchamp, D. M.; Kline, R. J.; Hammond, M. R.; McCulloch, I.; Heeney, M.; Ashraf, R. S.; Smith, J. N.; Anthopoulos, T. D.; Schroeder, B.; Geerts, Y. H.; Fischer, D. A.; Toney, M. F. *J. Am. Chem. Soc.* **2011**, *133*, 15073.
(40) Fazzi, D.; Caironi, M.; Castiglioni, C. *J. Am. Chem. Soc.* **2011**, *133*, 19056.
(41) Salleo, A.; Kline, R. J.; DeLongchamp, D. M.; Chabinyc, M. L. *Adv. Mater.* **2010**, *22*, 3812.